INTERNATIONAL JOURNAL FOR NUMERICAL METHODS IN FLUIDS
Int. J. Numer. Meth. Fluids 2006; **52**:433–453
Published online 10 February 2006 in Wiley InterScience (www.interscience.wiley.com). DOI: 10.1002/fld.1186

Riemann solvers with evolved initial conditions

E. F. Toro*,†

Laboratory of Applied Mathematics, Department of Civil and Environmental Engineering, University of Trento, Trento, Italy

SUMMARY

The scope of this paper is three fold. We first formulate upwind and symmetric schemes for hyperbolic equations with non-conservative terms. Then we propose upwind numerical schemes for conservative and non-conservative systems, based on a Riemann solver, the initial conditions of which are evolved non-linearly in time, prior to a simple linearization that leads to closed-form solutions. The Riemann solver is easily applied to complicated hyperbolic systems. Finally, as an example, we formulate conservative schemes for the three-dimensional Euler equations for general compressible materials and give numerical results for a variety of test problems for ideal gases in one and two space dimensions. Copyright © 2006 John Wiley & Sons, Ltd.

KEY WORDS: hyperbolic systems; non-conservative terms; Riemann problem; evolution of data; linearized Riemann solver; Euler equations; general equation of state; numerical results

1. INTRODUCTION

We are concerned with numerical methods for solving non-linear systems of hyperbolic equations. In particular, we are interested in designing numerical schemes for problems that involve non-conservative differential terms. In this paper we first formulate upwind and symmetric schemes by extending the finite volume approach. For the upwind schemes one requires intercell fluxes and intercell vector functions, the latter being associated with non-conservative differential terms. To compute these intercell quantities we then propose a Riemann solver for non-conservative systems. The Riemann solver consists of first evolving the initial conditions in time using the full non-linear system and then performing a simple linearization

*Correspondence to: E. F. Toro, Laboratory of Applied Mathematics, Department of Civil and Environmental Engineering, University of Trento, Trento, Italy.
†E-mail: toro@ing.unitn.it, www.ing.unitn.it/toro

Contract/grant sponsor: Isaac Newton Institute for Mathematical Sciences; contract/grant number: GR N09276
Contract/grant sponsor: Italian Ministry of Higher Education and Research

Received 17 August 2005
Revised 17 November 2005
Accepted 20 November 2005

of the Riemann problem, for which a straightforward solution can be obtained. The scheme may be interpreted in the framework of the MUSTA predictor–corrector approach [1–3] with the linearized Riemann solver as the corrector. The resulting first-order Godunov schemes are extended to second-order of accuracy in space and time under a TVD constraint to control spurious oscillations near large gradients. The second-order schemes are then extended to non-Cartesian two-dimensional geometries. The new Riemann solver is applied to the three-dimensional Euler equations with a general equation of state. The explicit solution is given. The associated numerical methods are partially validated by means of five test problems for which there are exact solutions, reference solutions or experimental data. Preliminary numerical results show that the proposed schemes are accurate, robust and efficient.

The rest of this paper is structured as follows. In Section 2 we formulate numerical schemes for hyperbolic equations that contain non-conservative differential terms. In Section 3 we present a new Riemann solver. In Section 4 we apply the Riemann solver to the three-dimensional Euler equations with general equations of state and present the explicit solution of the Riemann problem; numerical results for five test problems are presented. The main points of the paper are summarized in Section 5.

2. NUMERICAL SCHEMES

There are applications in which the governing equations cannot be written strictly in conservation-law form, or divergence form. Examples include models for compressible multi-phase flows. It is therefore of interest to study numerical methods for hyperbolic equations expressed in *quasi-conservative* form, namely

$$\partial_t \mathbf{Q} + \partial_x \mathbf{F}(\mathbf{Q}) + \partial_y \mathbf{G}(\mathbf{Q}) + \partial_z \mathbf{H}(\mathbf{Q}) + \mathbf{A}\partial_x \bar{\mathbf{F}}(\mathbf{Q}) + \mathbf{B}\partial_y \bar{\mathbf{G}}(\mathbf{Q}) + \mathbf{C}\partial_z \bar{\mathbf{H}}(\mathbf{Q}) = \mathbf{S}(\mathbf{Q}) \tag{1}$$

Here $\mathbf{Q}$ is the vector of unknowns, which for most problems of physical interest are the set of physically conserved variables. $\mathbf{F}(\mathbf{Q})$, $\mathbf{G}(\mathbf{Q})$ and $\mathbf{H}(\mathbf{Q})$ may be interpreted as physical fluxes in the x, y and z directions, respectively. The non-conservative terms involve coefficient matrices $\mathbf{A}(\mathbf{Q})$, $\mathbf{B}(\mathbf{Q})$, $\mathbf{C}(\mathbf{Q})$ and partial derivatives of the vector functions $\bar{\mathbf{F}}(\mathbf{Q})$, $\bar{\mathbf{G}}(\mathbf{Q})$ and $\bar{\mathbf{H}}(\mathbf{Q})$. $\mathbf{S}(\mathbf{Q})$ is a vector of source or forcing terms and does not involve derivatives of the unknowns.

In this section we formulate numerical schemes for solving equations of form (1).

2.1. Conservative systems

We first consider the simpler case of an $m \times m$ system of hyperbolic conservation laws

$$\partial_t \mathbf{Q} + \partial_x \mathbf{F}(\mathbf{Q}) = \mathbf{S}(\mathbf{Q}) \tag{2}$$

for which the finite volume approach applied on a control volume $[x_{i-1/2}, x_{i+1/2}] \times [t^n, t^{n+1}]$ yields

$$\mathbf{Q}_i^{n+1} = \mathbf{Q}_i^n - \frac{\Delta t}{\Delta x}[\mathbf{F}_{i+1/2} - \mathbf{F}_{i-1/2}] + \Delta t \mathbf{S}_i \tag{3}$$

where

$$\mathbf{Q}_i^n = \frac{1}{\Delta x}\int_{x_{i-1/2}}^{x_{i+1/2}} \mathbf{Q}(x,t)\,\mathrm{d}x$$

$$\mathbf{F}_{i+1/2} = \frac{1}{\Delta t}\int_{t^n}^{t^{n+1}} \mathbf{F}(\mathbf{Q}(x_{i+1/2},t))\,\mathrm{d}t \tag{4}$$

$$\mathbf{S}_i = \frac{1}{\Delta t}\frac{1}{\Delta x}\int_{t^n}^{t^{n+1}}\int_{x_{i-1/2}}^{x_{i+1/2}} \mathbf{S}(x,t,\mathbf{Q}(x,t))\,\mathrm{d}x\,\mathrm{d}t$$

with $\Delta x = x_{i+1/2} - x_{i-1/2}$ and $\Delta t = t^{n+1} - t^n$. These finite volume relations are exact. A finite volume numerical method results once approximations to $\mathbf{F}_{i+1/2}$ and $\mathbf{S}_i$ are provided, giving rise to numerical fluxes and numerical sources, respectively, denoted again by $\mathbf{F}_{i+1/2}$ and $\mathbf{S}_i$. Thus we interpret (3) as a finite volume numerical method to solve (2).

The following discussion concerns the definition of intercell numerical fluxes, for which there are two main approaches. Godunov's upwind approach [4] defines the intercell numerical flux $\mathbf{F}_{i+1/2}$ in terms of the similarity solution $\mathbf{Q}_{i+1/2}(x/t)$ of the Riemann problem

$$\partial_t \mathbf{Q} + \partial_x \mathbf{F}(\mathbf{Q}) = \mathbf{0}$$

$$\mathbf{Q}(x,0) = \begin{cases} \mathbf{Q}_i^n & \text{if } x < 0 \\ \mathbf{Q}_{i+1}^n & \text{if } x > 0 \end{cases} \tag{5}$$

The solution in the half-plane $t > 0$, $-\infty < x < +\infty$ forms the so-called *Riemann fan* which consists of $m+1$ constant states separated by m wave families, each one associated with a real eigenvalue $\lambda^{(k)}$. The Godunov intercell numerical flux is found by first evaluating $\mathbf{Q}_{i+1/2}(x/t)$ at $x/t = 0$, that is along the (local) t-axis, and then evaluating the physical flux vector $\mathbf{F}(\mathbf{Q})$ in (2) at $\mathbf{Q}_{i+1/2}(0)$, namely

$$\mathbf{F}_{i+1/2}^{\mathrm{God}} = \mathbf{F}(\mathbf{Q}_{i+1/2}(0)) \tag{6}$$

The exact solution will generally involve at least one iterative procedure and thus in practice, whenever possible, one uses approximate Riemann solvers. For a review on Riemann solvers see, for example, Reference [5].

Non-upwind (or centred, or symmetric) schemes, on the other hand, do not explicitly utilize wave propagation information and are thus simpler and more generally applicable. Examples are the Lax–Friedrichs flux, the two-step Lax–Wendroff flux [6] and the FORCE flux [7, 8]. One can introduce a minimum of wave propagation information into the framework of existing symmetric schemes. A well-known example is the Rusanov flux [9], sometimes also known as the *local* Lax–Friedrichs flux. Consider *local* mesh dimensions δt, δx and a local maximum wave speed

$$S_{i+1/2} = S_{i+1/2}(\mathbf{Q}_i^n, \mathbf{Q}_{i+1}^n)$$

that depends only on the data states left and right of the interface. For example, for the Euler equations one can set

$$S_{i+1/2} = \max(|u_i^n| + a_i^n, |u_{i+1}^n| + a_{i+1}^n) \tag{7}$$

where u_i^n and a_i^n are, respectively, particle velocity and sound speed in cell i at time level n. Similarly, u_{i+}^n and a_{i+1}^n are particle velocity and sound speed in cell $i+1$ at time level n.

The local mesh and local wave speed are related thus:

$$\frac{\delta x}{\delta t} = \frac{S_{i+1/2}}{\hat{C}_{\text{loc}}}$$

where C_{loc} is a prescribed CFL number for local use. Then, locally the classical Lax–Friedrichs flux can be written as

$$\mathbf{F}_{i+1/2}^{\text{LF}} = \frac{1}{2}\left[\mathbf{F}(\mathbf{Q}_i^n) + \mathbf{F}(\mathbf{Q}_{i+1}^n) - \frac{S_{i+1/2}}{C_{\text{loc}}}(\mathbf{Q}_{i+1}^n - \mathbf{Q}_i^n)\right] \tag{8}$$

Analogously, locally the Classical Lax–Wendroff flux becomes

$$\mathbf{F}_{i+1/2}^{\text{LW}} = \mathbf{F}(\mathbf{Q}_{i+1/2}^{\text{LW}}), \quad \mathbf{Q}_{i+1/2}^{\text{LW}} = \frac{1}{2}[\mathbf{Q}_i^n + \mathbf{Q}_{i+1}^n] - \frac{1}{2}\frac{C_{\text{loc}}}{S_{i+1/2}}[\mathbf{F}(\mathbf{Q}_{i+1}^n) - \mathbf{F}(\mathbf{Q}_i^n)] \tag{9}$$

The GFORCE numerical flux [10] is the weighted average

$$\mathbf{F}_{i+1/2}^{\text{GF}} = \Omega\mathbf{F}_{i+1/2}^{\text{LW}} + (1-\Omega)\mathbf{F}_{i+1/2}^{\text{LF}} \tag{10}$$

where

$$\Omega(C) = \frac{1}{1+C_{\text{loc}}} \tag{11}$$

An analysis of (10) in terms of the model equation

$$\partial_t q + \lambda \partial_x q = 0 \tag{12}$$

shows that for $C_{\text{loc}} = 1$ and $C_{\text{loc}} = C_{\text{cfl}} \leqslant 1$, where C_{cfl} is the chosen CFL coefficient for the numerical scheme (3), the GFORCE flux reduces to the Godunov's upwind flux, which gives the monotone scheme with the smallest local truncation error. Moreover, for $0 < C_{\text{loc}} < C_{\text{cfl}}$ the scheme is monotone but more diffusive than the Godunov's method and for $C_{\text{cfl}} < C_{\text{loc}} < 1$ the scheme is non-monotone. We use GFORCE with $C_{\text{loc}} = C_{\text{cfl}}$ or $C_{\text{loc}} = 1$.

2.2. *Quasi-conservative systems*

We consider hyperbolic equations of the form

$$\partial_t \mathbf{Q} + \partial_x \mathbf{F}(\mathbf{Q}) + \mathbf{A}(\mathbf{Q})\partial_x \bar{\mathbf{F}}(\mathbf{Q}) = \mathbf{S}(\mathbf{Q}) \tag{13}$$

As done for the derivation of the conservative scheme (3), integration of equations (13) over a control volume produces the following numerical scheme for the non-conservative system (13):

$$\mathbf{Q}_i^{n+1} = \mathbf{Q}_i^n - \frac{\Delta t}{\Delta x}[\mathbf{F}_{i+1/2} - \mathbf{F}_{i-1/2}] - \frac{\Delta t}{\Delta x}\mathbf{A}_i[\bar{\mathbf{F}}_{i+1/2} - \bar{\mathbf{F}}_{i-1/2}] + \Delta t \mathbf{S}_i \tag{14}$$

where $\mathbf{Q}_i^n$, $\mathbf{F}_{i+1/2}$, $\bar{\mathbf{F}}_{i+1/2}$ and $\mathbf{S}_i$ are approximations to the corresponding integral averages (4) and the coefficient matrix $\mathbf{A}_i$ is an approximation to a space-time integral of the matrix in the considered control volume, analogous to the numerical source $\mathbf{S}_i$ in (4).

Remark
There are various ways of obtaining an approximation leading to the coefficient matrix $\mathbf{A}_i$ in (14). In Reference [11] we explored approximations for the particular case in which the system was written in fully non-conservative form, that is when $\mathbf{F}(\mathbf{Q}) = \mathbf{0}$ in (13). The assessment of these approximations for the quasi-conservative case (13) is still a pending task. For discontinuous solutions, the choice may have an effect on the waves speeds.

Upwind-based approximations require the solution of the Riemann problem for the quasi-conservative system (13) to find the appropriate intercell approximations in scheme (14). This is the subject of Section 3.

A symmetric scheme to solve (13) is the following predictor–corrector scheme, in which the predictor step is:

$$\begin{aligned}\mathbf{Q}_{i-1/2}^{n+1/2} = {} & \frac{1}{2}(\mathbf{Q}_{i-1}^{n} + \mathbf{Q}_{i}^{n}) - \frac{1}{2}\frac{\Delta t}{\Delta x}[\mathbf{F}(\mathbf{Q}_{i}^{n}) - \mathbf{F}(\mathbf{Q}_{i-1}^{n})] \\ & - \frac{1}{2}\frac{\Delta t}{\Delta x}\mathbf{A}_{i-1/2}^{n}[\bar{\mathbf{F}}(\mathbf{Q}_{i}^{n}) - \bar{\mathbf{F}}(\mathbf{Q}_{i-1}^{n})] + \frac{1}{2}\Delta t\mathbf{S}_{i-1/2}\end{aligned} \tag{15}$$

and

$$\begin{aligned}\mathbf{Q}_{i+1/2}^{n+1/2} = {} & \frac{1}{2}(\mathbf{Q}_{i}^{n} + \mathbf{Q}_{i+1}^{n}) - \frac{1}{2}\frac{\Delta t}{\Delta x}[\mathbf{F}(\mathbf{Q}_{i+1}^{n}) - \mathbf{F}(\mathbf{Q}_{i}^{n})] \\ & - \frac{1}{2}\frac{\Delta t}{\Delta x}\mathbf{A}_{i+1/2}^{n}[\bar{\mathbf{F}}(\mathbf{Q}_{i+1}^{n}) - \bar{\mathbf{F}}(\mathbf{Q}_{i}^{n})] + \frac{1}{2}\Delta t\mathbf{S}_{i+1/2}\end{aligned} \tag{16}$$

The corrector step gives the solution in cell i at the new time level $n+1$ as

$$\begin{aligned}\mathbf{Q}_{i}^{n+1} = {} & \frac{1}{2}(\mathbf{Q}_{i-1/2}^{n+1/2} + \mathbf{Q}_{i+1/2}^{n+1/2}) - \frac{1}{2}\frac{\Delta t}{\Delta x}[\mathbf{F}(\mathbf{Q}_{i+1/2}^{n+1/2}) - \mathbf{F}(\mathbf{Q}_{i-1/2}^{n+1/2})] \\ & - \frac{1}{2}\frac{\Delta t}{\Delta x}\mathbf{A}_{i}^{n+1/2}[\bar{\mathbf{F}}(\mathbf{Q}_{i+1/2}^{n+1/2}) - \bar{\mathbf{F}}(\mathbf{Q}_{i-1/2}^{n+1/2})] + \frac{1}{2}\Delta t\mathbf{S}_{i}^{n+1/2}\end{aligned} \tag{17}$$

The coefficient matrices are taken as

$$\begin{aligned}\mathbf{A}_{i-1/2}^{n} &= \mathbf{A}(\tfrac{1}{2}(\mathbf{Q}_{i-1}^{n} + \mathbf{Q}_{i}^{n})) \\ \mathbf{A}_{i+1/2}^{n} &= \mathbf{A}(\tfrac{1}{2}(\mathbf{Q}_{i}^{n} + \mathbf{Q}_{i+1}^{n})) \\ \mathbf{A}_{i}^{n+1/2} &= \mathbf{A}(\tfrac{1}{2}(\mathbf{Q}_{i-1/2}^{n+1/2} + \mathbf{Q}_{i+1/2}^{n+1/2}))\end{aligned} \tag{18}$$

while the numerical sources are

$$\begin{aligned}\mathbf{S}_{i-1/2}^{n} &= \mathbf{S}(\tfrac{1}{2}(\mathbf{Q}_{i-1}^{n} + \mathbf{Q}_{i}^{n})) \\ \mathbf{S}_{i+1/2}^{n} &= \mathbf{S}(\tfrac{1}{2}(\mathbf{Q}_{i}^{n} + \mathbf{Q}_{i+1}^{n})) \\ \mathbf{S}_{i}^{n+1/2} &= \mathbf{S}(\tfrac{1}{2}(\mathbf{Q}_{i-1/2}^{n+1/2} + \mathbf{Q}_{i+1/2}^{n+1/2}))\end{aligned} \tag{19}$$

Scheme (15)–(17) does not require upwind information or knowledge of the eigenstructure of the system. In the next section we deal with upwind-based schemes of type (14).

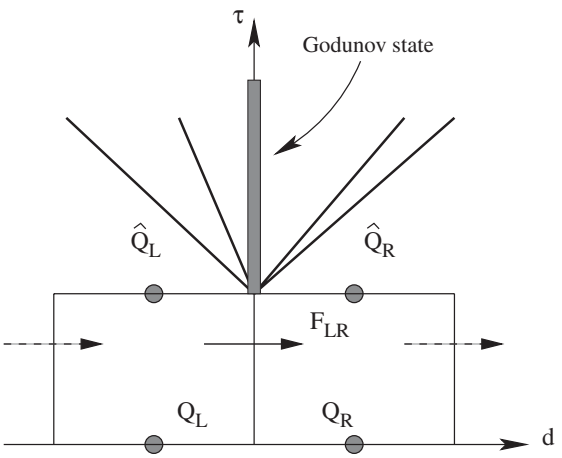

Figure 1. Illustration of the EVILIN scheme. First, the given states either side of the interface are evolved using the full non-linear equations. Then, the evolved states form the initial conditions for a simple linearized Riemann problem, whose solution is used to evaluate a Godunov flux.

3. THE EVILIN FLUX

Our aim is to provide a numerical flux by solving, approximately, the Riemann problem with *evolved* initial conditions

$$\partial_t \mathbf{Q} + \partial_x \mathbf{F}(\mathbf{Q}) + \mathbf{A}(\mathbf{Q})\partial_x \bar{\mathbf{F}}(\mathbf{Q}) = \mathbf{0}$$

$$\mathbf{Q}(x,0) = \begin{cases} \hat{\mathbf{Q}}_L & \text{if } x < 0 \\ \hat{\mathbf{Q}}_R & \text{if } x > 0 \end{cases} \tag{20}$$

to obtain a similarity solution $\hat{\mathbf{Q}}_{LR}(x/t)$ to be used in the computation of intercell numerical fluxes and intercell numerical functions in (14). It is important to realize that the initial conditions $\hat{\mathbf{Q}}_L, \hat{\mathbf{Q}}_R$ in (20) are assumed to have undergone a non-linear evolution step, as in the MUSTA approach [1–3].

Given that we EVolve the Initial conditions and then LINearize the Riemann problem, we call the scheme the EVILIN Riemann solver. The computation of the EVILIN flux has two main steps. These are illustrated in Figure 1.

3.1. Data evolution

A crucial step of the method is the time evolution of the initial conditions for (20), which has the effect of transforming *large* data $\mathbf{Q}_L, \mathbf{Q}_R$ to *small* data $\hat{\mathbf{Q}}_L, \hat{\mathbf{Q}}_R$. For a strictly conservative system, $\mathbf{A}(\mathbf{Q}) = \mathbf{0}$ in (20), the initial data are evolved as follows:

$$\hat{\mathbf{Q}}_L = \mathbf{Q}_L - \frac{\delta t}{\delta x}[\mathbf{F}_{LR} - \mathbf{F}(\mathbf{Q}_L)], \quad \hat{\mathbf{Q}}_R = \mathbf{Q}_R - \frac{\delta t}{\delta x}[\mathbf{F}(\mathbf{Q}_R) - \mathbf{F}_{LR}] \tag{21}$$

Here $\mathbf{F}_{LR} = \mathbf{F}_{LR}(\mathbf{Q}_L, \mathbf{Q}_R)$ is a numerical flux, δx is a given *local mesh size* and δt is a *local time step* determined from the data states $\mathbf{Q}_L, \mathbf{Q}_R$, the length δx and the *local* CFL coefficient C_{loc}. See (11) and definitions proceeding it. To compute $\mathbf{F}_{LR}$ we use the numerical flux function $\mathbf{F}^{GF}_{i+1/2}$ given by (10), (11).

For a quasi-conservative system, as in (20), we apply the procedure (15)–(17). The initial conditions of (20) are evolved as follows:

$$\begin{aligned}
\hat{\mathbf{Q}}_L &= \frac{1}{2}(\mathbf{Q}_L + \mathbf{Q}^{1/2}_{LR}) - \frac{1}{2}\frac{\delta t}{\delta x}[\mathbf{F}(\mathbf{Q}^{1/2}_{LR}) - \mathbf{F}(\mathbf{Q}_L)] - \frac{1}{2}\frac{\delta t}{\delta x}\mathbf{A}^{1/2}_L[\bar{\mathbf{F}}(\mathbf{Q}^{1/2}_{LR}) - \bar{\mathbf{F}}(\mathbf{Q}_L)] \\
\hat{\mathbf{Q}}_R &= \frac{1}{2}(\mathbf{Q}^{1/2}_{LR} + \mathbf{Q}_R) - \frac{1}{2}\frac{\delta t}{\delta x}[\mathbf{F}(\mathbf{Q}_R) - \mathbf{F}(\mathbf{Q}^{1/2}_{LR})] - \frac{1}{2}\frac{\delta t}{\delta x}\mathbf{A}^{1/2}_R[\bar{\mathbf{F}}(\mathbf{Q}_R) - \bar{\mathbf{F}}(\mathbf{Q}^{1/2}_{LR})]
\end{aligned} \tag{22}$$

where

$$\begin{aligned}
\mathbf{Q}^{1/2}_{LR} &= \frac{1}{2}(\mathbf{Q}_L + \mathbf{Q}_R) - \frac{1}{2}\frac{\delta t}{\delta x}[\mathbf{F}(\mathbf{Q}_R) - \mathbf{F}(\mathbf{Q}_L)] - \frac{1}{2}\frac{\delta t}{\delta x}\mathbf{A}_{LR}[\bar{\mathbf{F}}(\mathbf{Q}_R) - \bar{\mathbf{F}}(\mathbf{Q}_L)] \\
\mathbf{A}_{LR} &= \mathbf{A}(\tfrac{1}{2}(\mathbf{Q}_L + \mathbf{Q}_R)) \\
\mathbf{A}^{1/2}_L &= \mathbf{A}(\tfrac{1}{2}(\mathbf{Q}_L + \mathbf{Q}^{1/2}_{LR})) \\
\mathbf{A}^{1/2}_R &= \mathbf{A}(\tfrac{1}{2}(\mathbf{Q}^{1/2}_{LR} + \mathbf{Q}_R))
\end{aligned} \tag{23}$$

3.2. The Riemann problem for evolved data

We first select a suitable set of variables $\mathbf{W} = \mathbf{M}\mathbf{Q}$ that renders the equations and their eigenstructure analysis as simple as possible. $\mathbf{M}$ is a suitable transformation matrix. The trivial choice $\mathbf{M} = \mathbf{I}$ leaves the system is terms of the original, possibly conserved, variables. In terms of new variables $\mathbf{W}$ the governing equations in (20) may be written in quasi-linear (non-conservative) form as

$$\partial_t \mathbf{W} + \mathbf{B}(\mathbf{W})\partial_x \mathbf{W} = \mathbf{0} \tag{24}$$

We assume that the system is hyperbolic, with real (possibly non-distinct) eigenvalues

$$\lambda_1(\mathbf{W}) \leqslant \lambda_2(\mathbf{W}) \leqslant \cdots \leqslant \lambda_m(\mathbf{W}) \tag{25}$$

and a corresponding complete set of *linearly independent* right eigenvectors

$$\mathbf{R}^{(1)}(\mathbf{W}), \mathbf{R}^{(2)}(\mathbf{W}), \ldots, \mathbf{R}^{(m)}(\mathbf{W}) \tag{26}$$

We assume also that the eigenvalues and right eigenvectors are known analytically or numerically.

We perform a local linearization of system (24) based on the arithmetic mean matrix

$$\hat{\mathbf{B}}_{LR} = \mathbf{B}(\tfrac{1}{2}(\hat{\mathbf{W}}_L + \hat{\mathbf{W}}_R)) \tag{27}$$

with $\hat{\mathbf{W}}_{\mathrm{L}} = \mathbf{M}\hat{\mathbf{Q}}_{\mathrm{L}}$ and $\hat{\mathbf{W}}_{\mathrm{R}} = \mathbf{M}\hat{\mathbf{Q}}_{\mathrm{R}}$. Then we solve exactly the linearized Riemann problem

$$\partial_t \mathbf{W} + \hat{\mathbf{B}}_{\mathrm{LR}} \partial_x \mathbf{W} = \mathbf{0}$$

$$\mathbf{W}(x,0) = \begin{cases} \hat{\mathbf{W}}_{\mathrm{L}} & \text{if } x < 0 \\ \hat{\mathbf{W}}_{\mathrm{R}} & \text{if } x > 0 \end{cases} \tag{28}$$

We denote the eigenvalues and eigenvectors of $\hat{\mathbf{B}}_{\mathrm{LR}}$ by

$$\hat{\lambda}_i = \lambda_i(\tfrac{1}{2}(\hat{\mathbf{W}}_{\mathrm{L}} + \hat{\mathbf{W}}_{\mathrm{R}})), \quad \hat{\mathbf{R}}^{(i)} = \mathbf{R}^{(i)}(\tfrac{1}{2}(\hat{\mathbf{W}}_{\mathrm{L}} + \hat{\mathbf{W}}_{\mathrm{R}})), \quad \text{for } i = 1, 2, \ldots, m \tag{29}$$

The similarity solution $\hat{\mathbf{W}}_{\mathrm{LR}}(x/t)$ of (28) is obtained from standard theory of hyperbolic systems with constant coefficients. See Reference [5, Section 2.3.3, Chapter 2]. By projecting the jump $\Delta\hat{\mathbf{W}} \equiv \hat{\mathbf{W}}_{\mathrm{R}} - \hat{\mathbf{W}}_{\mathrm{L}}$ in the initial condition onto the eigenvectors one finds the wave strengths $\hat{\alpha}_i$, $i = 1, 2, \ldots, m$, by solving the linear algebraic system

$$\hat{\alpha}_1 \hat{\mathbf{R}}^{(1)} + \hat{\alpha}_2 \hat{\mathbf{R}}^{(2)} + \cdots + \hat{\alpha}_m \hat{\mathbf{R}}^{(m)} = \Delta\hat{\mathbf{W}} \tag{30}$$

For some problems of practical interest, the closed-form solution of this linear algebraic system can be easily obtained *by hand*. For more complicated systems we recommend the use of algebraic manipulators. One may also find the solution numerically using any standard software for linear algebraic systems.

Having found the wave strengths $\hat{\alpha}_i$, one knows the solution everywhere in the half-plane $t > 0$, $-\infty < x < \infty$. We are interested in the solution at the particular point $x/t = 0$ to determine the intercell fluxes $\mathbf{F}_{i+1/2}$ and intercell functions $\bar{\mathbf{F}}_{i+1/2}$ in (14). We have

$$\hat{\mathbf{W}}_{\mathrm{LR}}(0) = \hat{\mathbf{W}}_{\mathrm{L}} + \sum_{\hat{\lambda}_i < 0} \hat{\alpha}_i \hat{\mathbf{R}}^{(i)} \tag{31}$$

or

$$\hat{\mathbf{W}}_{\mathrm{LR}}(0) = \hat{\mathbf{W}}_{\mathrm{R}} - \sum_{\hat{\lambda}_i > 0} \hat{\alpha}_i \hat{\mathbf{R}}^{(i)} \tag{32}$$

or

$$\hat{\mathbf{W}}_{\mathrm{LR}}(0) = \frac{1}{2}(\hat{\mathbf{W}}_{\mathrm{L}} + \hat{\mathbf{W}}_{\mathrm{R}}) - \frac{1}{2}\sum_{i=1}^{m} \mathrm{sign}(\hat{\lambda}_i)\hat{\alpha}_i \hat{\mathbf{R}}^{(i)} \tag{33}$$

The sought intercell fluxes and intercell functions for use in (14) are

$$\mathbf{F}_{i+1/2} = \mathbf{F}(\hat{\mathbf{W}}_{\mathrm{LR}}(0)), \quad \bar{\mathbf{F}}_{i+1/2} = \bar{\mathbf{F}}(\hat{\mathbf{W}}_{\mathrm{LR}}(0)) \tag{34}$$

3.3. Summary of the scheme

The complete scheme is summarized into the following four steps

- *Evolution*: For each interface, evolve the initial conditions left and right according to (21) or (22). Note that this data evolution step has no relation with certain evolution procedures to obtain second order of accuracy, as in the MUSCL-Hancock method, for instance.

- *Choice of variables for linearization*: Select a suitable vector **W** of variables to perform the linearization of the Riemann problem, see (28).
- *Solution of linear Riemann problem*: Evaluate the Godunov state according to any of (31)–(33).
- *Numerical flux*: Evaluate the numerical fluxes and functions according to (34).

In the next section we apply the EVILIN Riemann solver to the Euler equations.

4. EXAMPLE: THE EULER EQUATIONS FOR GENERAL MATERIALS

The EVILIN method of this paper is most easily applied to any hyperbolic system for which the eigenstructure is known, analytically or numerically. In this section we demonstrate the performance of the schemes for a conservative system, namely the Euler equations for compressible materials.

4.1. Governing equations

The Euler equations in three space dimensions are

$$\partial_t \mathbf{Q} + \partial_x \mathbf{F}(\mathbf{Q}) + \partial_y \mathbf{G}(\mathbf{Q}) + \partial_z \mathbf{H}(\mathbf{Q}) = \mathbf{0} \tag{35}$$

with

$$\mathbf{Q} = \begin{bmatrix} \rho \\ \rho u \\ \rho v \\ \rho w \\ E \end{bmatrix}, \quad \mathbf{F}(\mathbf{Q}) = \begin{bmatrix} \rho u \\ \rho u^2 + p \\ \rho uv \\ \rho uw \\ u(E+p) \end{bmatrix}, \quad \mathbf{G}(\mathbf{Q}) = \begin{bmatrix} \rho v \\ \rho vu \\ \rho v^2 + p \\ \rho vw \\ v(E+p) \end{bmatrix}, \quad \mathbf{H}(\mathbf{Q}) = \begin{bmatrix} \rho w \\ \rho wu \\ \rho wv \\ \rho w^2 + p \\ w(E+p) \end{bmatrix} \tag{36}$$

Here ρ is density; u, v and w are velocity components in the x, y and z directions, respectively; p is pressure and E is total energy given by

$$E = \rho[\tfrac{1}{2}(u^2 + v^2 + w^2) + e] \tag{37}$$

with e being the specific internal energy.

To have a determined system one requires a closure condition. For general compressible materials one uses a caloric equation of state relating the variables ρ, p and e. Often one uses other variables, such as the specific volume $1/\rho$ and the entropy s. Here we consider two possible functional relations for a general equilibrium equation of state in terms of the variables ρ, p and e. These are given below, along with the corresponding expressions for the sound speed in the considered material

$$p = p(\rho, e) \to a = \sqrt{\frac{p}{\rho^2} p_e + p_\rho}, \quad e = e(\rho, p) \to a = \sqrt{\frac{p}{\rho^2 e_p} - \frac{e_\rho}{e_p}} \tag{38}$$

where subscripts denote partial derivatives. We assume the standard convexity condition for the equation of state. For the simple case of ideal gases one has the familiar equation of state and corresponding sound speed

$$e = \frac{p}{(\gamma - 1)\rho} \rightarrow a = \sqrt{\frac{\gamma p}{\rho}} \tag{39}$$

where γ is the ratio of specific heats. For air under most conditions one takes $\gamma = 1.4$. General background on thermodynamics and equations of state can be found, for example, in Reference [12] and references therein.

4.2. The PVRS Riemann solver with evolved data

In the frame of finite volume schemes one requires a numerical flux in the direction normal to each volume face, at each integration point. Thus, without loss of generality, to find the intercell flux we may consider the split augmented one-dimensional problem in the x direction. Here we generalize the so-called PVRS Riemann solver, first proposed in Reference [13], and apply it with initial data that have been evolved, as suggested in Section 3.1. We choose the physical or primitive variable vector $\mathbf{W} = [\rho, u, v, w, p]^{\mathrm{T}}$ to work with. Then

$$\partial_t \mathbf{W} + \mathbf{B}(\mathbf{W})\partial_x \mathbf{W} = \mathbf{0} \tag{40}$$

with

$$\mathbf{W} = \begin{bmatrix} \rho \\ u \\ v \\ w \\ p \end{bmatrix}, \quad \mathbf{B}(\mathbf{W}) = \begin{bmatrix} u & \rho & 0 & 0 & 0 \\ 0 & u & 0 & 0 & \frac{1}{\rho} \\ 0 & 0 & u & 0 & 0 \\ 0 & 0 & 0 & u & 0 \\ 0 & \rho a^2 & 0 & 0 & u \end{bmatrix} \tag{41}$$

The real eigenvalues are

$$\lambda_1 = u - a, \quad \lambda_2 = \lambda_3 = \lambda_4 = u, \quad \lambda_5 = u + a \tag{42}$$

with corresponding right eigenvectors

$$\mathbf{R}^{(1)} = \begin{bmatrix} -\rho/a \\ 1 \\ 0 \\ 0 \\ -\rho a \end{bmatrix}, \quad \mathbf{R}^{(2)} = \begin{bmatrix} 1 \\ 0 \\ 0 \\ 0 \\ 0 \end{bmatrix}, \quad \mathbf{R}^{(3)} = \begin{bmatrix} 0 \\ 0 \\ 1 \\ 0 \\ 0 \end{bmatrix}, \quad \mathbf{R}^{(4)} = \begin{bmatrix} 0 \\ 0 \\ 0 \\ 1 \\ 0 \end{bmatrix}, \quad \mathbf{R}^{(5)} = \begin{bmatrix} \rho/a \\ 1 \\ 0 \\ 0 \\ \rho a \end{bmatrix} \tag{43}$$

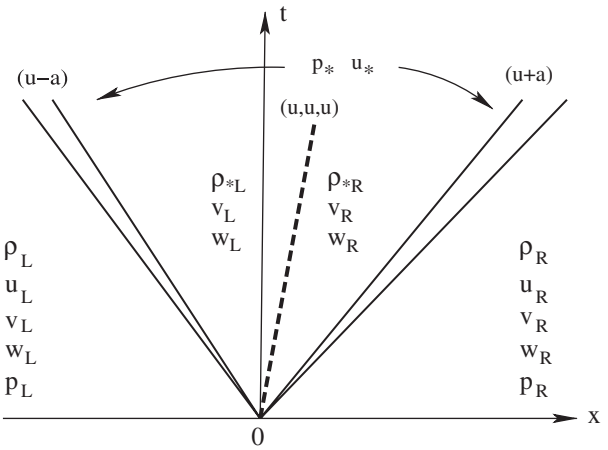

Figure 2. Structure of the solution of the split three-dimensional Riemann problem *normal* to a cell interface for the Euler equations for compressible materials with a general convex equation of state.

We solve the Riemann problem

$$\partial_t \mathbf{W} + \mathbf{B}(\mathbf{W})\partial_x \mathbf{W} = \mathbf{0}$$

$$\mathbf{W}(x,0) = \begin{cases} \hat{\mathbf{W}}_{\mathrm{L}} \equiv \mathbf{M}\hat{\mathbf{Q}}_{\mathrm{L}} & \text{if } x < 0 \\ \hat{\mathbf{W}}_{\mathrm{R}} \equiv \mathbf{M}\hat{\mathbf{Q}}_{\mathrm{R}} & \text{if } x > 0 \end{cases} \tag{44}$$

where $\hat{\mathbf{Q}}_{\mathrm{L}}$ and $\hat{\mathbf{Q}}_{\mathrm{R}}$ are evolved initial conditions using the non-linear step (21) or (22).

The structure of the solution of the normal Riemann problem is depicted in Figure 2. The multiple eigenvalue $\lambda = u$ is associated with a contact discontinuity, a shear wave in the y direction and a shear wave in the z direction. There are four constant regions. The region of unknowns is called the *Star Region*, which is divided by the contact wave into a *Star Left* and a *Star Right* regions.

The linear algebraic system (30) has solution

$$\begin{aligned} \hat{\alpha}_1 &= \frac{1}{2}\frac{\Delta p - \Delta u \tilde{\rho}\tilde{a}}{\tilde{\rho}\tilde{a}^2} \\ \hat{\alpha}_2 &= \frac{\Delta \rho \tilde{a}^2 - \Delta p}{\tilde{a}^2} \\ \hat{\alpha}_3 &= \Delta v \\ \hat{\alpha}_4 &= \Delta w \\ \hat{\alpha}_5 &= \frac{1}{2}\frac{\Delta p + \Delta u \tilde{\rho}\tilde{a}}{\tilde{\rho}\tilde{a}^2} \end{aligned} \tag{45}$$

where $\Delta q = \hat{q}_R - \hat{q}_L$, for any component q of the vector of unknowns $\mathbf{W}$. The linearization requires mean values $\tilde{q}$ for the components q, for which we take the simple arithmetic means $\tilde{q} = 1/2(\hat{q}_L + \hat{q}_R)$. The explicit solution in the unknown *Star Region*, see Figure 2, is given by

$$\begin{aligned} p^* &= \tfrac{1}{2}(\hat{p}_L + \hat{p}_R) - \tfrac{1}{2}(\hat{u}_R - \hat{u}_L)C_1 \\ u^* &= \tfrac{1}{2}(\hat{u}_L + \hat{u}_R) - \tfrac{1}{2}(\hat{p}_R - \hat{p}_L)/C_1 \\ \rho_L^* &= \hat{\rho}_L + (\hat{u}_L - u^*)C_2 \\ \rho_R^* &= \hat{\rho}_R + (u^* - \hat{u}_R)C_2 \\ v_L^* &= \hat{v}_L \\ v_R^* &= \hat{v}_R \\ w_L^* &= \hat{w}_L \\ w_R^* &= \hat{w}_R \end{aligned} \tag{46}$$

where

$$C_1 = \tilde{\rho}\tilde{a}, \quad C_2 = \tilde{\rho}/\tilde{a} \tag{47}$$

To completely determine the solution we also need to specify estimates for the partial derivatives e_ρ and e_p in the general equation of state (38) in order to evaluate $\tilde{a}$. We suggest

$$\tilde{e}_\rho = \tfrac{1}{2}[(e_\rho)_L + (e_\rho)_R], \quad \tilde{e}_p = \tfrac{1}{2}[(e_p)_L + (e_p)_R] \tag{48}$$

where $(e_\rho)_L$, $(e_\rho)_R$, $(e_p)_L$, $(e_p)_R$ are evaluated on the *evolved* states $\hat{\mathbf{W}}_L$, $\hat{\mathbf{W}}_R$, respectively. For the ideal gas case $\tilde{a} = \sqrt{\gamma \tilde{p}/\tilde{\rho}}$, as expected.

Remarks
Solution (46) is valid for any equation of state of form (38), which enters the solution via the data-evolution step and via the speed of sound in the constants C_1 and C_2 in (47). The approximate solution (46) of the Riemann problem is *complete*, in the sense that accounts for all waves present in the structure of the exact solution of the non-linear Riemann problem. This has a bearing on the resolution capability of the associated Godunov scheme, particularly for the linearly degenerate fields. We note also that the given solution for density and shear waves, the linearly degenerate fields, has the same structure as the exact solution, the only approximation being that for the *normal* particle speed u^*. Note that the solution for these waves is exact if the initial data are connected by a corresponding isolated wave, provided the tangential velocity components have not undergone a predictor step. In practice, it seems as if the resolution of shear waves is not affected by applying the predictor step also to the tangential velocity components. However, this may be the subject of some further study.

4.3. Sample numerical results

We illustrate the performance of the EVILIN Riemann solver proposed in this paper as applied to the time-dependent Euler equations in one space dimension and in two space dimensions

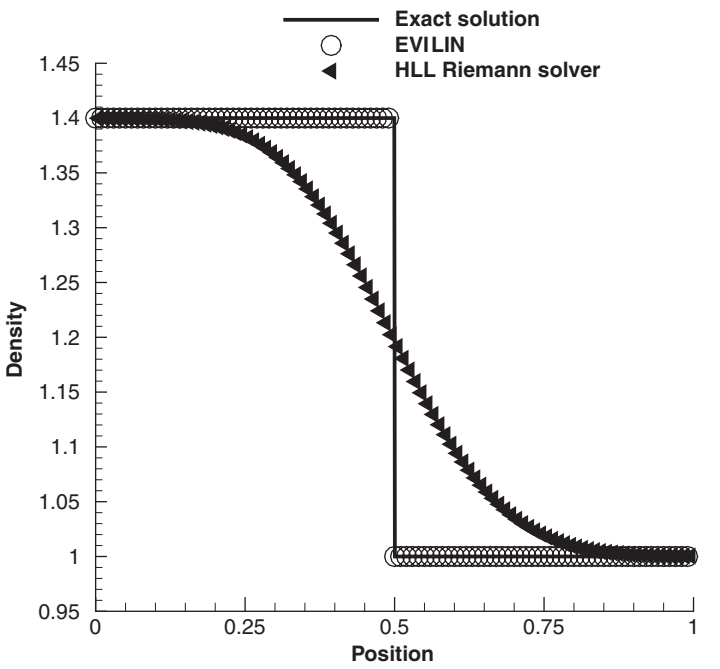

Figure 3. *Test* 1: *Stationary contact*. EVILIN and HLL results (first-order) for density are compared with the exact solution (full line) at time $t = 2.0\,\text{ms}$ with $M = 100$ cells.

on non-Cartesian geometries. We use the ideal gas equation of state with constant gamma, $\gamma = 1.4$. We compare results with exact solutions and with reference solutions. We consider five test problems, for all of which we use a CFL coefficient $C_{\text{cfl}} = 0.9$ for the computations.

4.3.1. Test 1: *stationary contact.* We solve the equations in a domain $[0, 1]$. The initial condition consists of constant pressure $p = 1$, constant velocity $u = 1$ and a discontinuous distribution of density: $\rho = 1.4$ in $[0, 1/2]$ and $\rho = 1.0$ in $(1/2, 1]$. We apply transmissive boundary condition at both ends. The purpose is to assess the performance of EVILIN for resolving *delicate features*, such as contact discontinuities, for which most numerical methods have large numerical dissipation, being the largest for the case in which the wave is stationary.

In Figure 3 we compare numerical results with the exact solution. As is illustrated by the HLL [14] result (triangles), non-complete Riemann solvers have large numerical dissipation for linearly degenerated fields. The proposed EVILIN Riemann solver reproduces the exact solution (circles).

4.3.2. Test 2: *shock-tube problem with sonic flow.* Here we assess EVILIN for a shock-tube problem with *sonic flow*. We solve the problem in the domain $[0, 1]$, subdivided into a left section $[0, 0.3]$ and a right section $(0.3, 1]$. The initial conditions assign data for density, velocity and pressure $\rho_{\text{L}} = 1.0$, $u_{\text{L}} = 3/4$, $p_{\text{L}} = 1.0$ in the left section and $\rho_{\text{R}} = 1/8$, $u_{\text{R}} = 0.0$,

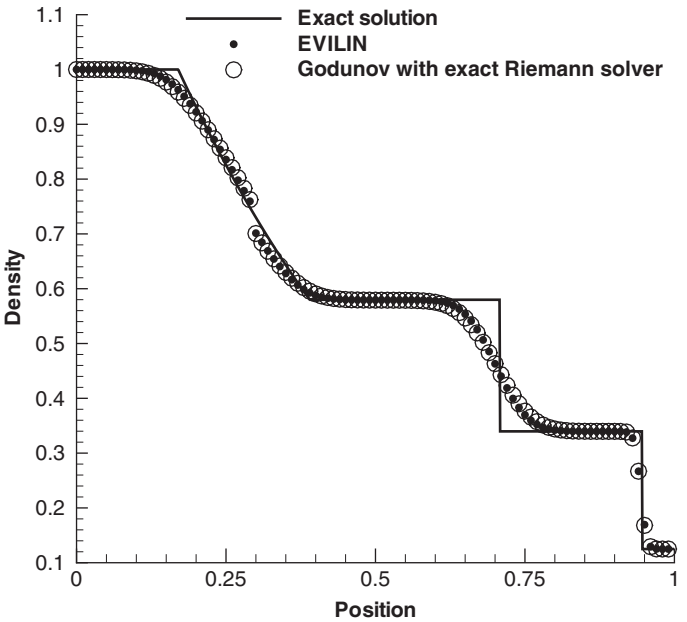

Figure 4. *Test* 2: *Shock tube with sonic flow*. EVILIN result (first-order) for density is compared with the exact solution (full line) at time $t = 0.30$ ms with $M = 100$ cells.

$p_R = 0.1$ in the right section. The solution includes a right shock, a right contact discontinuity and a left *transonic*, or *sonic* rarefaction wave. We remark that this is not the original Sod test problem but a modification of it so as to produce a transonic rarefaction as part of the solution. The *sonic point* is known to cause difficulties to numerical methods. Conventional linearized Riemann solvers give a large jump in all flow variables, a *rarefaction shock*, unless explicit *entropy fixes* are enforced.

Figure 4 shows numerical results for density as compared with the exact solution. The numerical results from the Godunov method with the exact Riemann solver and those from EVILIN are virtually indistinguishable, particularly for the shock and for the sonic point. It is well known that the exact Riemann solver, although theoretically entropy satisfying, produces a visible *entropy glitch* at the sonic point. The EVILIN solver also produces this small glitch but the method has no *ad hoc* entropy fixes, which are essential for all classical linearized Riemann solvers available. We observe that the size of this small entropy jump is seen to tend to zero as the mesh is refined, for both EVILIN and for the exact Riemann solver.

4.3.3. Test 3: *low-density flow.* Here we assess EVILIN for a shock-tube problem with *low-density flow*. We solve a Riemann problem in the domain $[0, 1]$, subdivided into a left section $[0, 1/2]$ and a right section $(1/2, 1]$. The initial conditions consists of constant density $\rho = 1$, constant pressure $p = 0.4$ and a discontinuous distribution of velocity $u_L = -2$ in $[0, 1/2]$ and $u_R = 2$ in $(1/2, 1.0]$. The solution consists of two strong symmetric rarefaction waves with stationary flow in the middle. This is a difficult test for many numerical methods. In particular,

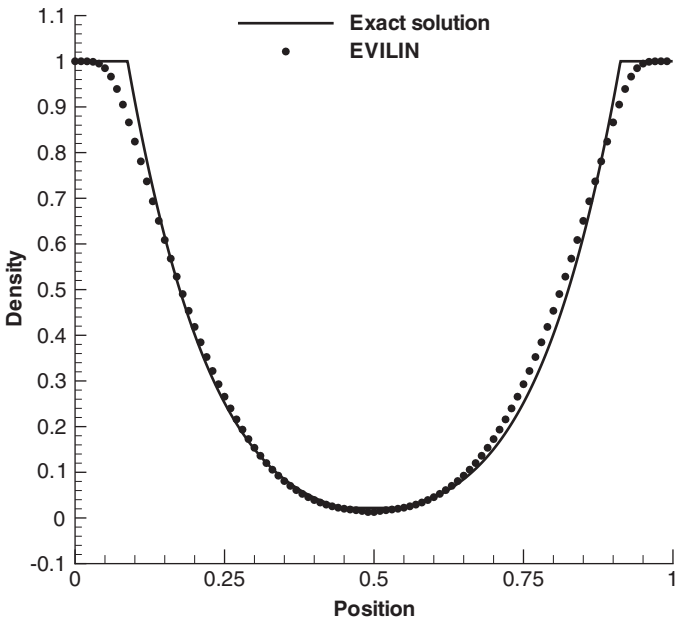

Figure 5. *Test* 3: *Low-density flow*. EVILIN result (first-order) for density is compared with the exact solution (full line) at time $t = 0.15$ ms with $M = 100$ cells.

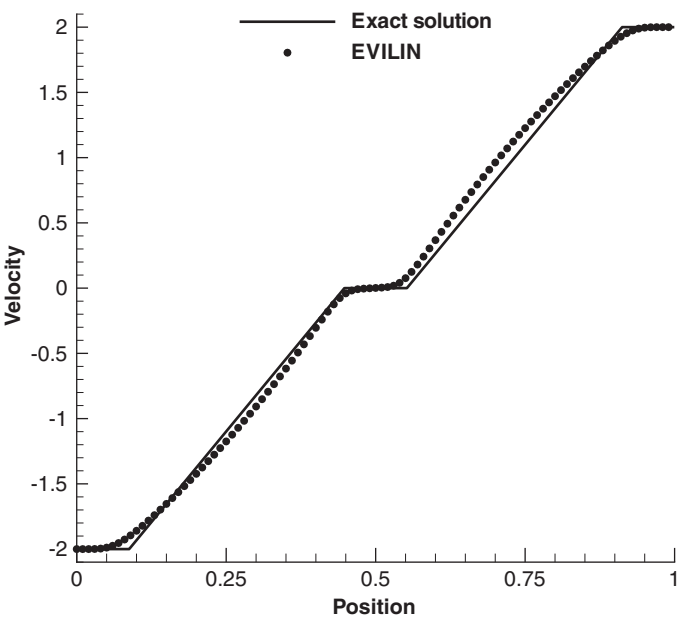

Figure 6. *Test* 3: *Low-density flow*. EVILIN result (first-order) for velocity is compared with the exact solution (full line) at time $t = 0.15$ ms with $M = 100$ cells.

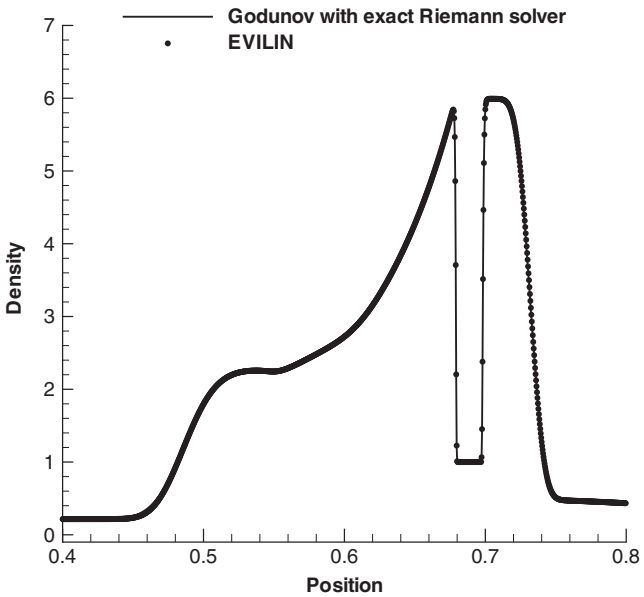

Figure 7. *Test* 4: *Blast wave problem*. Results (first-order) from EVILIN and the Godunov scheme with the exact Riemann solver (full line) at time $t = 0.027\,\text{ms}$ with $M = 3000$ cells.

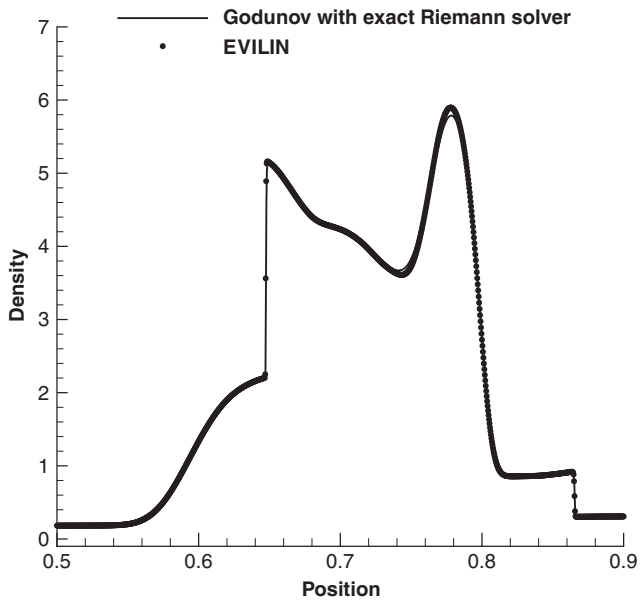

Figure 8. *Test* 4: *Blast wave problem*. Results (first-order) from EVILIN and the Godunov scheme with the exact Riemann solver (full line) at time $t = 0.038\,\text{ms}$ with $M = 3000$ cells.

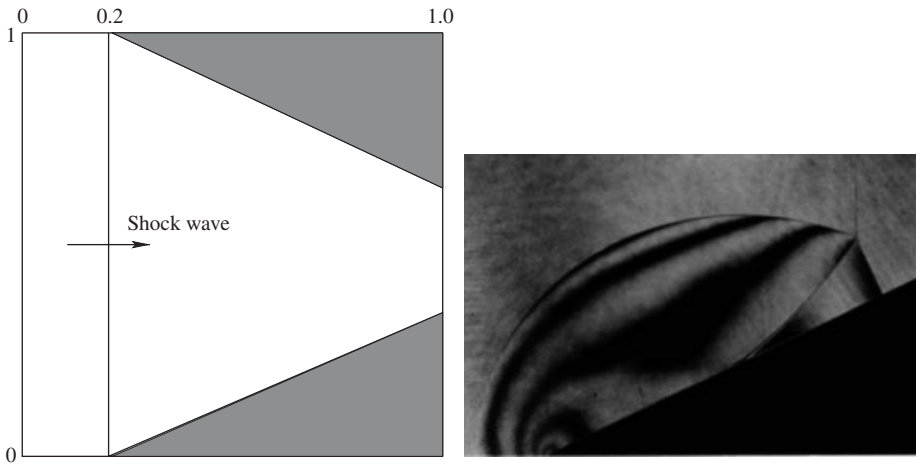

Figure 9. *Test* 5: *Mach reflection problem*. Left-hand side sketch shows computational domain and position of initial shock wave. Right-hand side picture shows the experimental result for the lower half of the domain (Courtesy Prof. K Takayama, Japan).

it is known that conventional linearized Riemann solvers [15] produce negative pressures and negative densities, leading the codes to crush.

Figures 5 and 6 compare numerical results against the exact solution, for density and velocity, respectively. We remark that the region of stationary flow, see Figure 6, is difficult to resolve, even for well-established complete Riemann solvers, such as HLLC [16]. EVILIN gives an accurate solution there, particularly for the stationary region.

4.3.4. Test 4: *blast wave interaction.* We solve the equations in a domain $[0,1]$. The initial condition consists of constant density $\rho = 1$, constant velocity $u = 0$ and a discontinuous distribution of pressure: $p_{\mathrm{L}} = 1000$ in $[0, 1/10]$, $p_{\mathrm{M}} = 0.01$ in $(1/10, 9/10]$ and $p_{\mathrm{R}} = 100$ in $(9/10, 1]$. For a detailed discussion on the solution of this problem see Reference [17]. The purpose of this test is to assess the robustness and accuracy of the present Riemann solver for resolving very strong shock waves and multiple wave–wave and wave–boundary interactions.

Figures 7 and 8 compare numerical results for density from EVILIN with those from the Godunov scheme with the exact Riemann solver for two output times. Figure 7 shows the case just before the collision of two very strong shock waves emerging from the discontinuous initial conditions. The results from EVILIN and the exact Riemann solver are indistinguishable. Figure 8 shows the solution after multiple wave interaction. The result from EVILIN agrees well with that from the exact Riemann solver.

4.3.5. Test 5: *Mach reflection in two space dimensions.* This test consists of a shock reflection problem in a two-dimensional non-Cartesian domain as depicted by the left-hand side sketch of Figure 9. This is a double-wedge situation in which a plane shock wave travels from left to right, reflects from the wedges placed at an angle of 25° to the initial shock direction, producing a symmetric Mach reflection pattern. The right-hand side picture of Figure 9 shows

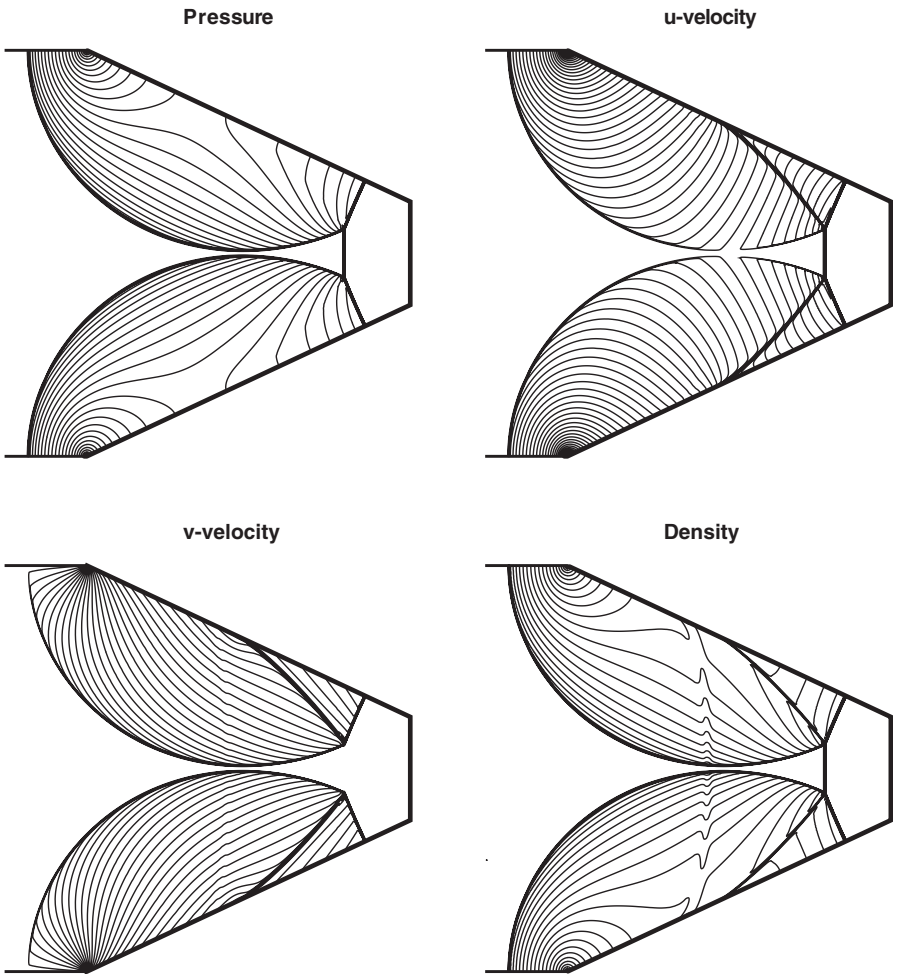

Figure 10. *Test* 5: *Mach reflection problem*. Numerical results (second-order) at time $t = 1.0\,\text{ms}$ for a mesh of 1000×1000 cells.

the experimental result for a single wedge, that is, the lower half of the domain shown on the left-hand side. Clearly seen in the experiment are the incident shock, the reflected shock, the Mach stem and the slip surface, all meeting at the triple point. The experiment corresponds to an initial shock wave of shock Mach number 1.7. Numerical results from a second-order TVD extension of EVILIN are given in Figures 10 and 11, in which contours are shown for 80 equally spaced levels.

Figure 10 shows computed results at the output time $t = 1.0\,\text{ms}$ using a mesh of $M = 1000 \times 1000$ cells. The qualitative agreement between the numerical solution and the experimental result of Figure 9 (right-hand side) is very satisfactory. All features seen in the experiment are reproduced in the numerical solution. The numerical results have also preserved the expected symmetry of the problem. Note also that our results do not escape the typical, so-called,

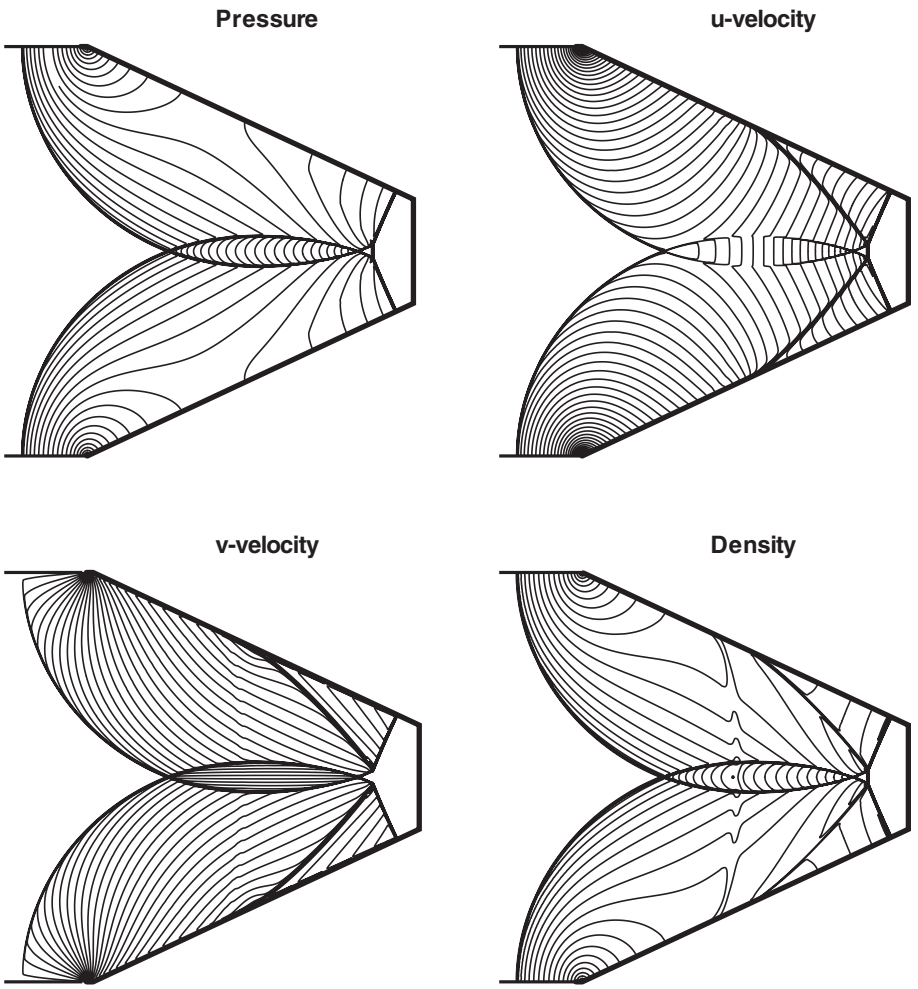

Figure 11. *Test* 5: *Mach reflection problem*. Numerical results (second-order) at time $t = 1.1$ ms for a mesh of 1000×1000 cells.

start-up error, which is clearly seen in the density plot. There are standard ways of eliminating this error.

The numerical resolution of all discontinuities is very satisfactory; discontinuities are sharp and free from spurious oscillations. For modern numerical methods the resolution of shocks is usually straightforward, but not so the resolution of linearly degenerate fields, for which one of the problems to be encountered is excessive numerical diffusion. Our results also show a sharp and oscillation-free resolution of the slip surface emanating from the triple point.

Finally, Figure 11 shows the numerical solution at time $t = 1.1$ ms. Note that the two reflected shock waves have interacted producing two new, stronger reflected shocks waves. This computation is included to demonstrate the ability of the scheme to handle strong wave interaction in multiple space dimensions.

5. SUMMARY

We have formulated upwind and symmetric schemes for non-linear hyperbolic systems containing non-conservative differential terms. The upwind schemes require the solution of the Riemann problem, for which we have proposed a new scheme in which one first evolves in time the initial conditions, non-linearly, and then performs a simple linearization of the Riemann problem, for which a straightforward solution can be obtained. The complete scheme is non-linear. The EVILIN method presented in this paper effectively extends the family of complete non-linear Riemann solvers to all hyperbolic systems for which the eigenstructure is known analytically or numerically.

For the conservative case we have illustrated the resulting upwind schemes for the three-dimensional Euler equations with general equation of state, have given the explicit solution of the Riemann problem and have shown numerical results for ideal gases for one- and two-dimensional problems, for first- and second-order non-linear schemes in non-Cartesian geometries.

Work in progress includes the application of the EVILIN Riemann solver in the framework of very high order finite volume ADER schemes to solve the equations of non-linear elasticity and the equations for compressible multi-phase flows. Preliminary results are very encouraging.

ACKNOWLEDGEMENTS

The initial part of this work was carried out while the author was an EPSRC senior visiting fellow (Grant GR N09276) at the Isaac Newton Institute for Mathematical Sciences, University of Cambridge, U.K., as joint organizer (with P. G. LeFloch and C. M. Dafermos) of the research programme *Non-linear Hyperbolic Waves in Phase Dynamics and Astrophysics*, Cambridge, January–July 2003. The support provided is gratefully acknowledged. Part of this work was also supported by a PRIN 2004 research grant from the Italian Ministry of Higher Education and Research.

I am also indebted to Dr Vladimir Titarev and Cristobal Castro, University of Trento, for useful discussions and comments.

REFERENCES

1. Toro EF. Multi-stage predictor–corrector fluxes for hyperbolic equations. *Technical Report NI03037-NPA*, Isaac Newton Institute for Mathematical Sciences, University of Cambridge, U.K., 17th June, 2003.
2. Toro EF. A multi-stage numerical flux. *Applied Numerical Mathematics*, 2005, in press.
3. Titarev VA, Toro EF. MUSTA schemes for multi-dimensional hyperbolic systems: analysis and improvements. *International Journal for Numerical Methods in Fluids* 2005; **49**:117–147.
4. Godunov SK. Finite difference methods for the computation of discontinuous solutions of the equations of fluid dynamics. *Matematicheskii Sbornik* 1959; **47**:271–306.
5. Toro EF. *Riemann Solvers and Numerical Methods for Fluid Dynamics* (2nd edn). Springer: Berlin, 1999.
6. Lax PD, Wendroff B. Systems of conservation laws. *Communications on Pure and Applied Mathematics* 1960; **13**:217–237.
7. Toro EF, Billett SJ. Centred TVD schemes for hyperbolic conservation laws. *IMA Journal of Numerical Analysis* 2000; **20**:47–79.
8. Chen GQ, Toro EF. Centred schemes for non-linear hyperbolic equations. *Journal of Hyperbolic Differential Equations* 2004; **1**(1):531–566.
9. Rusanov VV. Calculation of interaction of non-steady shock waves with obstacles. *Journal of Computational Mathematics and Physics USSR* 1961; **1**:267–279.
10. Toro EF, Titarev VA. MUSTA schemes for systems of conservation laws. *Technical Report NI04033-NPA*, Isaac Newton Institute for Mathematical Sciences, University of Cambridge, U.K., 2004.
11. Toro EF, Siviglia A. PRICE: primitive centred schemes for hyperbolic systems. *International Journal for Numerical Methods in Fluids* 2003; **42**:1263–1291.

12. Menikoff R, Plohr BJ. The Riemann problem for fluid flow of real materials. *Reviews of Modern Physics* 1989; **61**:75–130.
13. Toro EF. A linearised Riemann solver for the time-dependent Euler equations of gas dynamics. *Proceedings of the Royal Society of London Series A* 1991; **434**:683–693.
14. Harten A, Lax PD, van Leer B. On upstream differencing and Godunov-type schemes for hyperbolic conservation laws. *SIAM Review* 1983; **25**(1):35–61.
15. Einfeldt B, Munz CD, Roe PL, Sjögreen B. On Godunov-type methods near low densities. *Journal of Computational Physics* 1991; **92**:273–295.
16. Toro EF, Spruce M, Speares W. Restoration of the contact surface in the HLL-Riemann solver. *Shock Waves* 1994; **4**:25–34.
17. Woodward P, Colella P. The numerical simulation of two-dimensional fluid flow with strong shocks. *Journal of Computational Physics* 1984; **54**:115–173.

